Supplementary Materials for

Small reduction in land surface albedo due to solar panel expansion worldwide

Authors: Sihuan Wei[1], Alan D. Ziegler[2], Yingzuo Qin[1], Dashan Wang[1], Yuntian Chen[3], Jinyue Yan[4], Zhenzhong Zeng[1,*]

Affiliations:

[1] School of Environmental Science and Engineering, Southern University of Science and Technology, Shenzhen 518055, China.

[2] Faculty of Fisheries Technology and Aquatic Resources, Mae Jo University, Chiang Mai 50000, Thailand.

[3] Ningbo Institute of Digital Twin, Eastern Institute of Technology, Ningbo, Zhejiang 315200, China.

[4] Department of Building Environment and Energy Engineering, The Hong Kong Polytechnic University, Kowloon, Hong Kong, China.

[*]Corresponding author: Zhenzhong Zeng (zengzz@sustech.edu.cn)

This file includes:

Supplementary Methods

Local radiative forcing due to albedo change

At the global scale, radiative forcing reflects the energy balance of the entire Earth's atmospheric system, influenced by global climate change factors such as changes in atmospheric greenhouse gas concentrations and solar radiation intensity. Local radiative forcing focuses more on radiation imbalances within specific regions, often associated with local weather systems or topography. Here, assuming the constant atmospheric transmittance factor, the local (relative) radiative forcing caused by PV-induced albedo change is simply expressed as follows:

$$LRF_{\overline{\Delta Albedo}} = \frac{RF_{\overline{\Delta Albedo}} A_E}{A_{PV}} \tag{1}$$

where $RF_{\overline{\Delta Albedo}}$ is the global radiative forcing caused by PV-induced albedo change, A_{PV} represents the scope area covered by PV facilities in a PV site, A_E denotes the Earth's surface area (510 × 10^6 km^2).

Carbon avoidance from PV generation

Carbon avoidance (CA) is defined as the reduced carbon emissions each year from a PV site's generation per unit compared to coal-fired plants, which is written as follows:

$$CA = \frac{CE_{gen}}{A_{PV}} - 8760 \cdot \lambda \cdot LCA \cdot CF \cdot Cap \tag{2}$$

where CE_{gen} is the yearly reduced carbon emissions from the PV site's generation, compared to coal-fired plants. Additionally, 8,760 present the corresponding number of hours in a year. LCA is the life cycle carbon emission of PV installations, which is assumed as 0.026 kg C kWh^{-1} in this study[1].

Directly comparing the NPP differences

We compared the remotely sensed Net Primary Production (NPP) variations in space, to represent the influenced carbon sink of natural land surface caused by PV deployment. We downloaded annual NPP information from 2019 to 2021 from the MOD17A3HGF v061 product (available at https://lpdaac.usgs.gov/products/mod17a3hgfv061/), which provides data information at 500 m pixel. The linear parameterization method used for calculating albedo change is not suitable for estimating the NPP change because the regression result is not robust (Supplementary Fig. 23). In order to detect the PV-induced NPP change preliminary, we directly compared the NPP between a PV site and its corresponding buffer zone (with a width of 2 pixels; Supplementary Fig. 21). The PV-induced NPP change can be written as follows:

$$\Delta NPP = \overline{NPP}_{PV} - \overline{NPP}_{Buffer} \qquad (3)$$

where ΔGPP represents the mean NPP change caused by PV deployment, $\overline{NPP}_{PV}$ and $\overline{NPP}_{Buffer}$ are the 3-year averaged NPPs (2019-2021) in the PV site and buffer zone respectively.

Supplementary Table 1. Previous studies modeling the climate feedbacks from deploying solar panels on natural ground. The values enclosed in brackets represent the satellite-based shortwave albedo of the study area in modeling studies. With the exception of Chang *et al.*[5], whose study region aligns with one of our PV sites, the remaining values are only the mean albedo of 2019, aimed at minimizing computational burdens.

Scale	Model	Albedo		Albedo Change		Land Cover	Source
		Background	PV Site	Absolute	Relative		
[a]Global	UMD –ICTP	0.34 (0.3337)	0.1	-0.24	-71%	Desert	Li *et al.*[2]
[a]Global	EC-Earth	~0.2 to ~0.4 (0.3337)	0.1	~-0.1 to ~-0.3	~-50% to ~-75%	Desert	Lu *et al.*[3]
[a]Regional	WRF	~0.21 (0.2186)	0.05	~-0.16	~-76%	Desert	Millstein *et al.*[4]
Regional	[b]WRF	[c]0.38 [d]0.38	[c]0.16 [d]0.21	[c]-0.22 [d]-0.17	[c]58% [d]55%	Barren or Sparsely Vegetated	Chang *et al.*[5]
Regional	[b]WRF	[c]0.25 [d]0.30 (0.1915)	[c]0.13 [d]0.15 (0.1794)	[c]-0.12 [d]-0.15	[c]48% [d]50%	Shrubland	Chang *et al.*[6]

[a]: Assuming solar panels cover the interested place with 100 % coverage.

[b]: The background albedo values are found from look-up table.

[c]: Maximum albedo.

[d]: Minimum albedo.

Supplementary Table 2. The comparison of shortwave albedo between our study and other studies.

Longitude (°)	Latitude (°)	Satellite		In-situ observations		Land cover	Source
		Background	Change	Background	Change		
95.233	36.503	[a]0.2102	[a]-0.0162	0.26	-0.07	Barren	Yang *et al.*[7]
100.588	36.136	[a]0.1664	[a]-0.0216	0.179	0.005	Barren	Chang *et al.*[8]
-111.284	32.555	-	-	0.3	-0.09	Barren	Broadbent *et al.*[9]
119.793	32.303	-	-	0.101	-0.019	Water body	Li *et al.*[10]
87.660	44.410	[a]0.1916	[a]-0.0100	0.23	-0.09	Barren	Li *et al.*[11]
87.660	44.410	[a]0.1916	[a]-0.0100	[b]0.22	-0.08	Barren	Ying *et al.*[12]
35.059	29.965	-	-	0.38	-0.21	[c]Barren	Stern *et al.*[1]
94.250	40.000	[a]0.1905	[a]-0.0145	-	-	Barren	Hua *et al.*[13]
		0.2216	-0.0287	-	-		
[d]Comprehensive sites		-	[a]-0.024	-	-	-	Zhang *et al.*[14]
		-	-0.036	-	-	-	
[e]Comprehensive sites		-	[a]-0.0126	-	-	Grass-lands	Xu *et al.*[15]
		-	-0.014	-	-		
		-	[a]-0.0142	-	-	Barren	
		-	-0.025	-	-		
		-	[a]-0.0102	-	-	Crop-lands	
		-	-0.010	-	-		

[a]: Our study.

[b]: The background for comparison is not near the PV site.

[c]: This site is located in a typical desert land under hot and arid climate conditions.

[d]: Zhang *et al.*[14] selected 23 PV plants (1 km resolution satellite-based albedo data), but only 17 plants exist or have high accuracy in the PV dataset used in our study. In order to compare with their results, here the albedo change we calculated is the mean value of the 17 PV plants.

[f]: Xu *et al.*[15] selected 116 solar power plants (both PV and concentrated solar power (CSP) plants with area larger than four 1-km pixels to reduce the effect of mixed pixels) and only calculated the white-sky albedo. Here we didn't select the sites they used for a detailed comparison, but rather conducted a general albedo change comparison of sites over different land use types.

Supplementary Table 3. The absolute and relative albedo change of filtered sites covered by PV panels. Each category contains three kind of statistics, the first shows the number of sites, the second and third show the median (IQR) of the absolute albedo change ($\times10^{-2}$) and the relative albedo change (%), respectively.

Country	**Land-cover type**					
	Grasslands	**Croplands**	**Barren**	**Open Shrublands**	**Others**	**Total**
All	144	61	77	39	31	352
	-1.26 (-1.82, -0.86)	-1.02 (-1.39, -0.77)	-1.42 (-1.82, -1.01)	-1.51 (-2.17, -1.09)	-1.41 (-2.03, -0.95)	-1.28 (-1.80, -0.90)
	-7.3 (-10.4, -4.7)	-6.7 (-8.9, -5.1)	-6.6 (-8.6, -5.2)	-7.0 (-10.7, -6.2)	-12.5 (-15.9, -7.3)	-7.1 (-10.8, -5.0)
China	94	25	50	0	19	188
	-1.18 (-1.79, -0.80)	-0.96 (-1.22, -0.77)	-1.27 (-1.55, -0.97)	-	-1.62 (-2.03, -1.22)	-1.23 (-1.65, -0.84)
	-6.5 (-9.4, -4.2)	-6.5 (-7.9, -5.0)	-6.3 (-7.6, -4.6)	-	-13.5 (-17.0, -9.5)	-6.7 (-9.4, -4.7)
United States	26	4	7	22	8	67
	-1.74 (-2.16, -1.33)	-2.55 (-3.24, -2.04)	-2.58 (-3.15, -1.85)	-1.70 (-2.69, -1.31)	-0.54 (-1.45, 0.60)	-1.73 (-2.37, -1.31)
	-9.7 (-12.7, -7.2)	-14.9 (-17.5, -12.0)	-12.9 (-16.0, -11.3)	-8.8 (-12.7, -6.6)	-4.0 (-10.9, -0.7)	-9.8 (-13.1, -6.7)
India	8	14	4	4	0	30
	-1.38 (-1.75, -0.81)	-0.87 (-1.19, -0.57)	-1.89 (-2.70, -1.24)	-1.52 (-1.62, -1.32)	-	-1.15 (-1.62, -0.77)
	-8.6 (-10.1, -5.5)	-6.3 (-8.9, -4.7)	-8.1 (-12.1, -5.2)	-6.3 (-6.7, -6.3)	-	-6.5 (-9.2, -5.3)
Others	16	18	16	13	4	67
	-1.20 (-1.68, -1.14)	-1.08 (-1.35, -0.88)	-1.61 (-2.56, -1.01)	-1.15 (-1.38, -0.90)	-1.96 (-3.06, -1.23)	-1.19 (-1.70, -0.97)
	-8.1 (-11.1, -6.2)	-6.9 (-8.4, -5.7)	-7.5 (-13.8, -5.4)	-6.4 (-9.2, -4.4)	-15.7 (-21.2, -10.9)	-7.1 (-9.7, -5.7)

Supplementary Table 4. The albedo of PV sites over the same specific land cover under different climate conditions. Q25 and Q75 are 25th and 75th percent interval quantiles, respectively.

Type	Number of sites	Median	Q25	Q75
OS-BWh	14	0.1915	0.1784	0.2094
OS-BWk	7	0.1908	0.1854	0.1966
OS-BSk	5	0.1662	0.1488	0.1714
OS-Csa	13	0.1708	0.1474	0.1786
WSa-Cfb	3	0.1236	0.1139	0.1370
Sa-Cfb	12	0.1180	0.1051	0.1309
Gr-BWk	29	0.1731	0.1644	0.1877
Gr-BSk	9	0.1484	0.1333	0.1616
Gr-Csa	69	0.1604	0.1486	0.1717
Gr-Cfb	3	0.1265	0.1133	0.1375
Gr-Dwb	12	0.1488	0.1227	0.1585
Gr-Dwc	10	0.1600	0.1557	0.1642
Gr-Dfc	4	0.1250	0.1157	0.1623
Cr-Aw	11	0.1253	0.1197	0.1391
Cr-BWh	3	0.1788	0.1638	0.1813
Cr-BSk	5	0.1453	0.1306	0.1525
Cr-Csa	6	0.1561	0.1431	0.1810
Cr-Cwb	3	0.1398	0.1302	0.1441
Cr-Cfb	7	0.1234	0.1001	0.1363
Cr-Dwb	15	0.1442	0.1386	0.1492
Cr-Dfc	7	0.1443	0.1361	0.1504
Ba-BWh	15	0.1991	0.1648	0.2276
Ba-BWk	59	0.1867	0.1709	0.2037
WB-Cfb	3	0.0971	0.0861	0.1003
WB-Dwb	4	0.0805	0.0758	0.0938

Supplementary Table 5. Count of PV sites in various Köppen-Geiger climate regimes[16].

Climate regime	Number	Description
Aw	12	Tropical, savannah
BWh	34	Arid, desert, hot
BWk	95	Arid, desert, cold
BSh	19	Arid, steppe, hot
BSk	90	Arid, steppe, cold
Cwa	8	Temperate, dry winter, hot summer
Cfa	31	Temperate, no dry season, hot summer
Cfb	5	Temperate, no dry season, warm summer
Dwa	31	Cold, dry winter, hot summer
Dwb	11	Cold, dry winter, warm summer
Dwc	2	Cold, dry winter, cold summer
Dfa	2	Cold, no dry season, hot summer
Dfb	12	Cold, no dry season, very cold winter

Supplementary Table 6. Sensitivity test. Here, the criteria of the number of pixels in a domain and the difference between the maximum and minimum area ratio of the PV panel range to the corresponding pixel are changed to observe the sites left.

Number of filtered sites		Number of pixels						
		20	15	12	10	9	8	7
Max (AR) – Min (AR)	>0.3	190	283	361	425	461	498	529
	>0.4	189	282	360	422	456	489	513
	>0.5	188	279	353	412	444	470	488

Supplementary Table 7. Count of PV sites in various land-cover types.

Land-cover Type	Number	Land-cover Type	Number
Open Shrublands	39	Croplands	61
Woody Savannas	6	Cropland/Natural Vegetation Mosaics	3
Savannas	14	Barren	77
Grasslands	144	Water Bodies	7
Permanent Wetlands	1	-	-

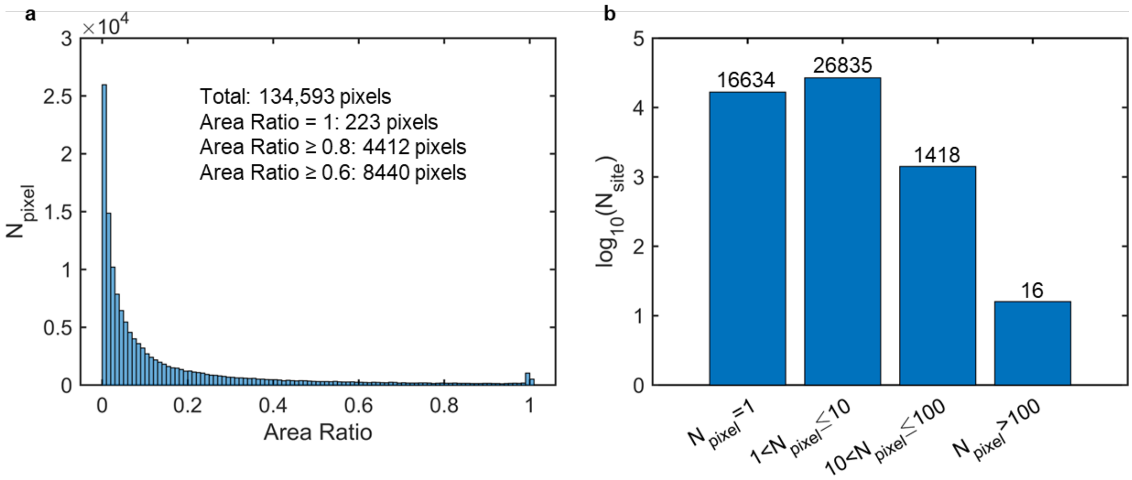

Supplementary Figure 1. The analysis of grid cells containing PV facilities. a, Histogram illustrating the count of pixels (N_{pixel}) with varying ratios of PV facilities' area to the corresponding grid area. **b**, Distribution of sites (N_{site}) based on the number of grid cells containing PV facilities (N_{pixel}).

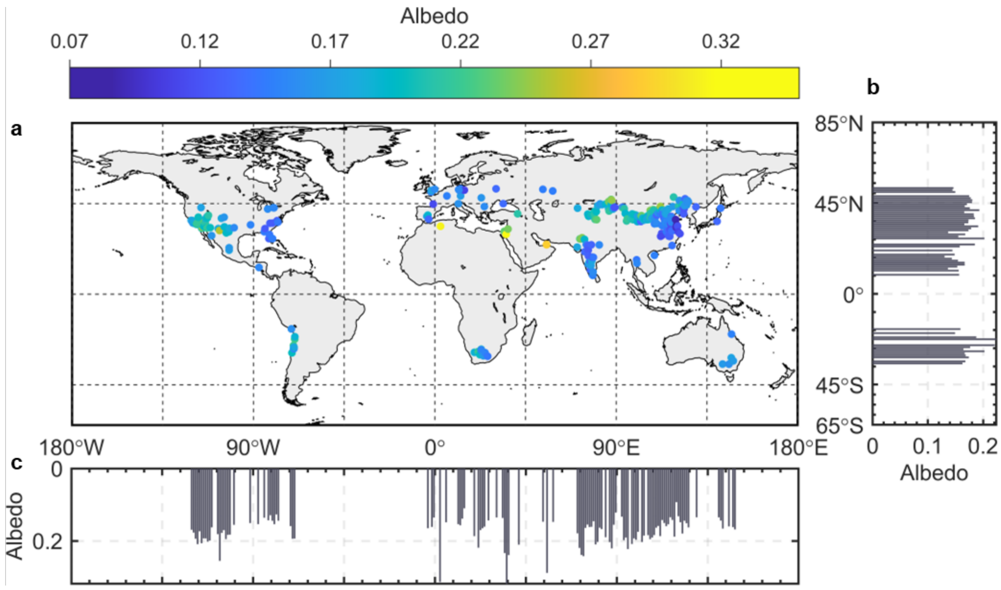

Supplementary Figure 2. The background albedo of 352 specific sites due to PV deployment. a, Spatial distribution of PV sites' albedo change. **b** and **c**, The latitude (**b**) and longitude (**c**) pattern of mean albedo change per degree.

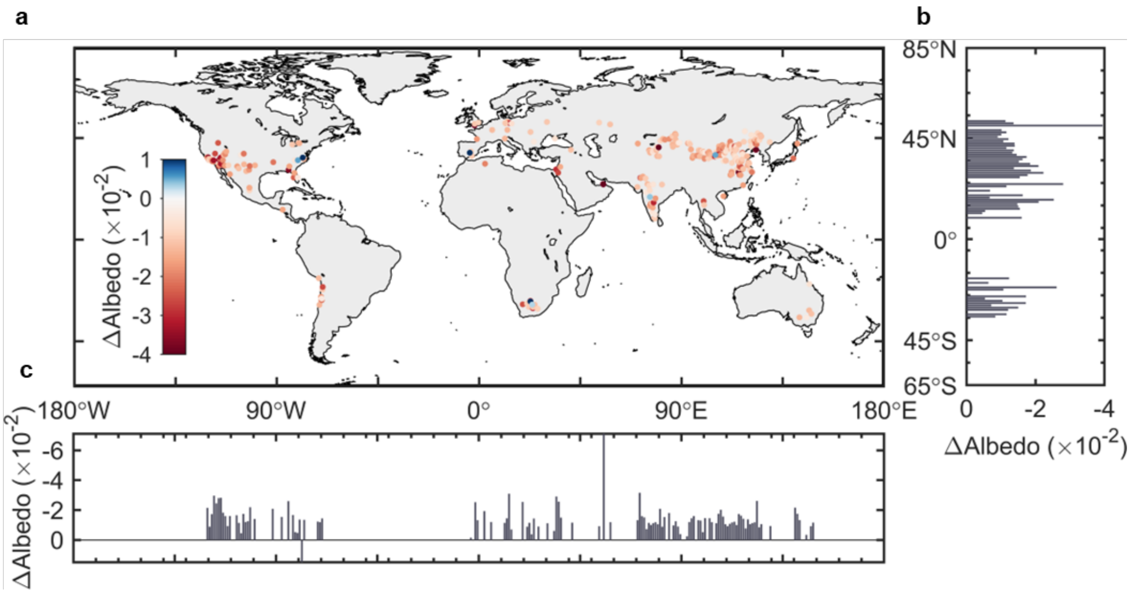

Supplementary Figure 3. The absolute albedo change (× 10^{-2}) of 352 specific sites due to PV deployment. a, Spatial distribution of PV sites' absolute albedo change. **b** and **c**, The latitude (**b**) and longitude (**c**) patterns of mean absolute albedo change per degree.

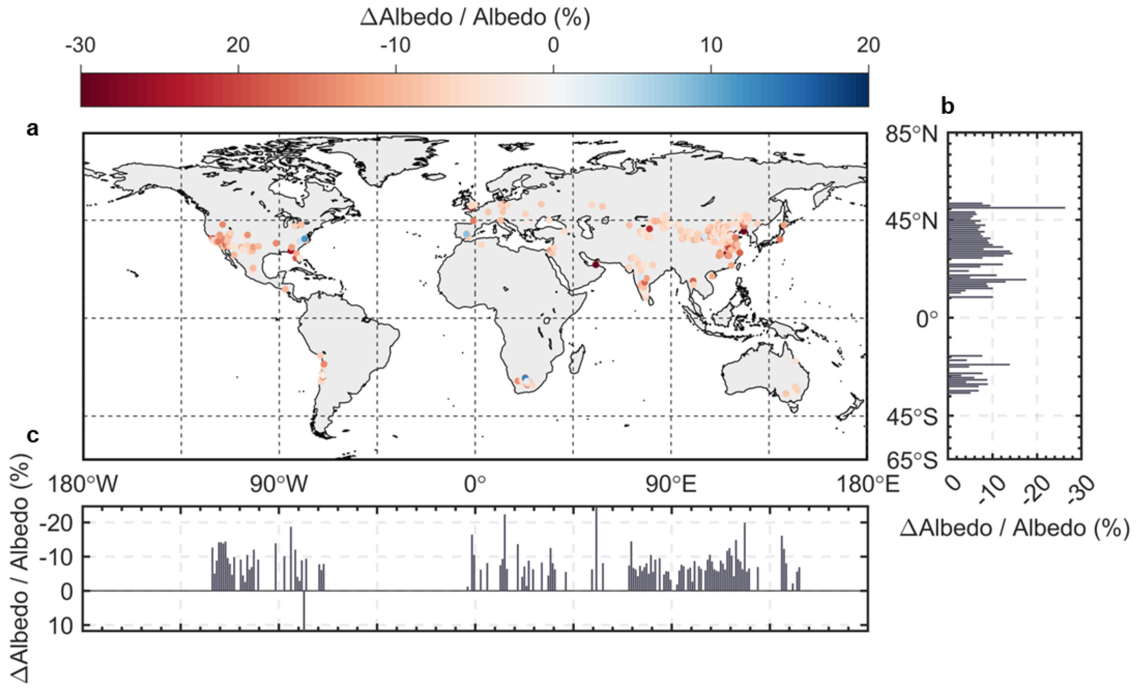

Supplementary Figure 4. The relative albedo change (%) of 352 specific sites due to PV deployment. a, Spatial distribution of PV sites' relative albedo change. **b** and **c**, The latitude (**b**) and longitude (**c**) patterns of mean relative albedo change per degree.

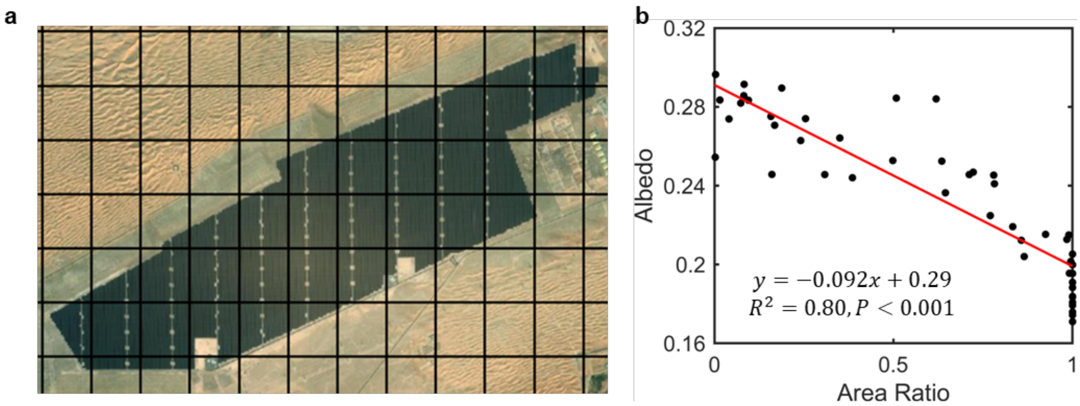

Supplementary Figure 5. Noor Abu Dhabi Solar Power Plant (55.44°E, 22.54°N), where maximum albedo reduction happens. In **a**, the satellite imagery is extracted from ERSI World Imagery (2022-1-12) in ArcMap 10.8. The grid cells have a resolution of 500 m. **b**, The correlation between area ratio and albedo. The solid red line denotes the fitting line.

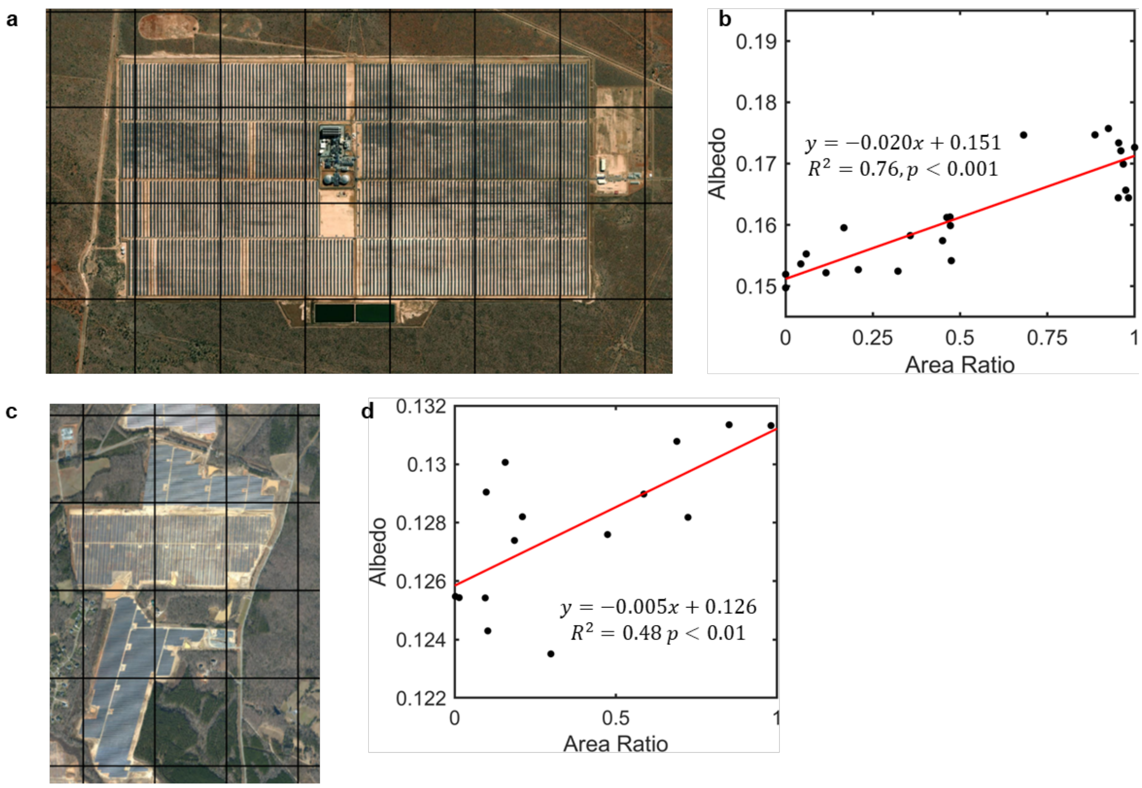

Supplementary Figure 6. Two sites with positive albedo change. In **a** (23.03°E, 27.61°S) and **c** (80.50°W, 35.30°N), The satellite imageries are extracted from ERSI World Imagery (2022-1-12) in ArcMap 10.8. The grid cells have a resolution of 500m. **b** and **d** show the linear regression and corresponding parameters. The solid red line denotes the fitting line.

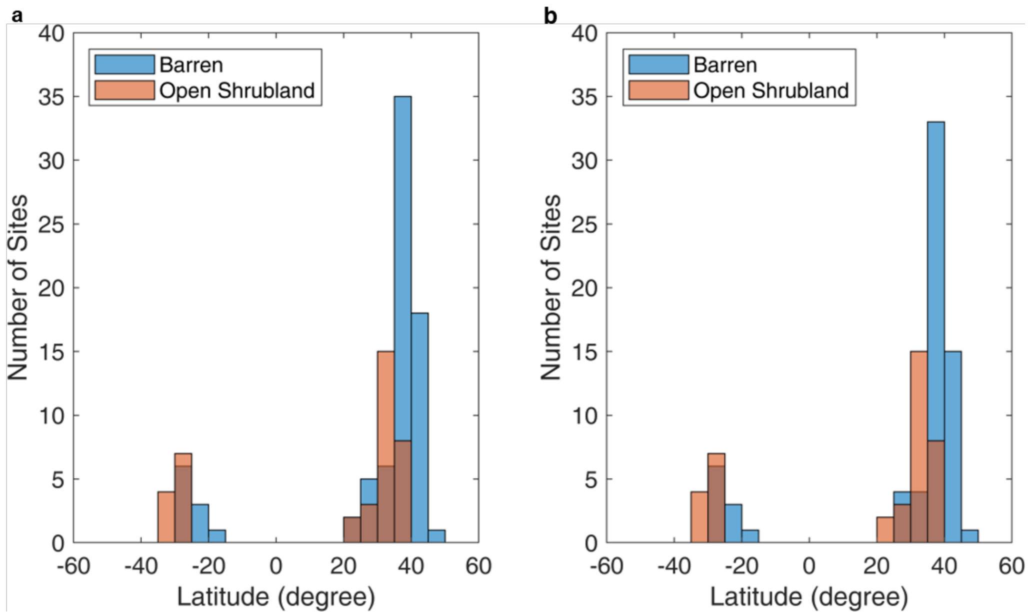

Supplementary Figure 7. The latitude pattern comparison of PV sites over open shrublands and barren. a, The latitude pattern of all PV sites over open shrublands (n = 39) and barren (n = 77). **b**, The latitude pattern of sites over open shrublands (n = 39) and filtered sites over barren (n = 67). The barren sites included in **b** have been selectively filtered to match the background albedo range of the open shrublands, ensuring a consistent comparison of background albedo between the two land cover types. Most of the PV sites located over barren (38.99°N; median) are positioned at higher latitudes compared to those over open shrublands (34.06°N; median) in the Northern Hemisphere. This implies that PV arrays at these barren sites require greater spacing to mitigate the shading effects on the panel generation.

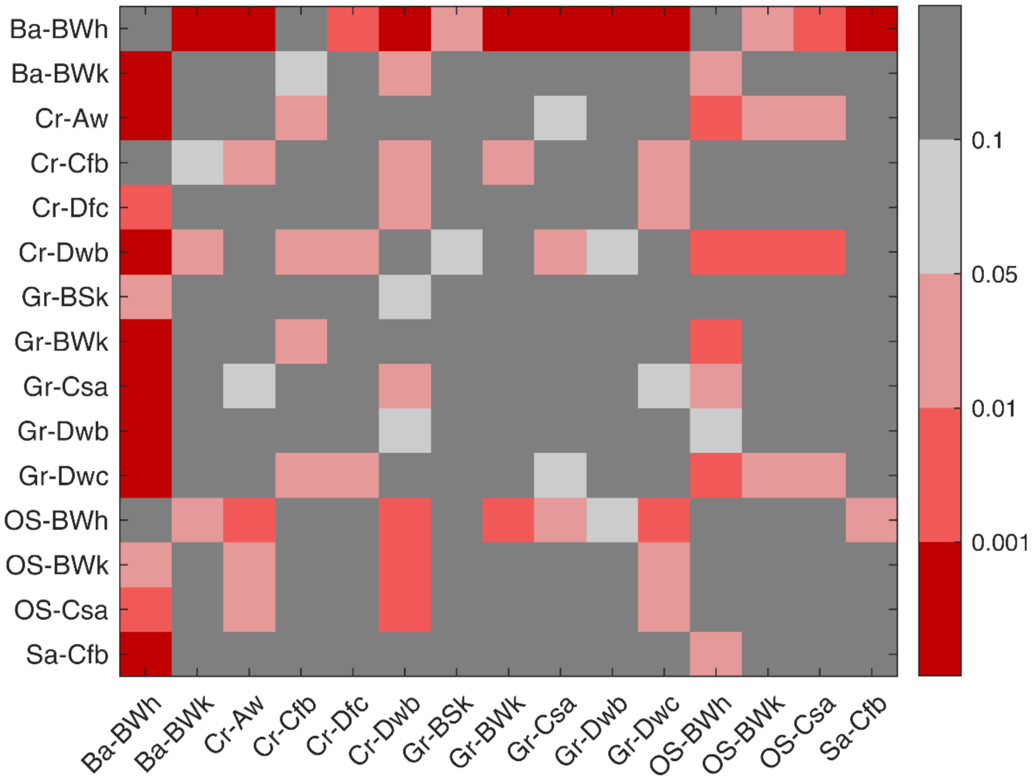

Supplementary Figure 8. The significant-difference-level of albedo change between sites in climate regimes of corresponding land-cover types. Wilcoxon rank sum test is used (* $P < 0.05$, ** $P < 0.01$, *** $P < 0.001$). Only categories with a site number greater than 7 are shown here. For further clarification on the abbreviations used for the climate regimes, please refer to Supplementary Table 5.

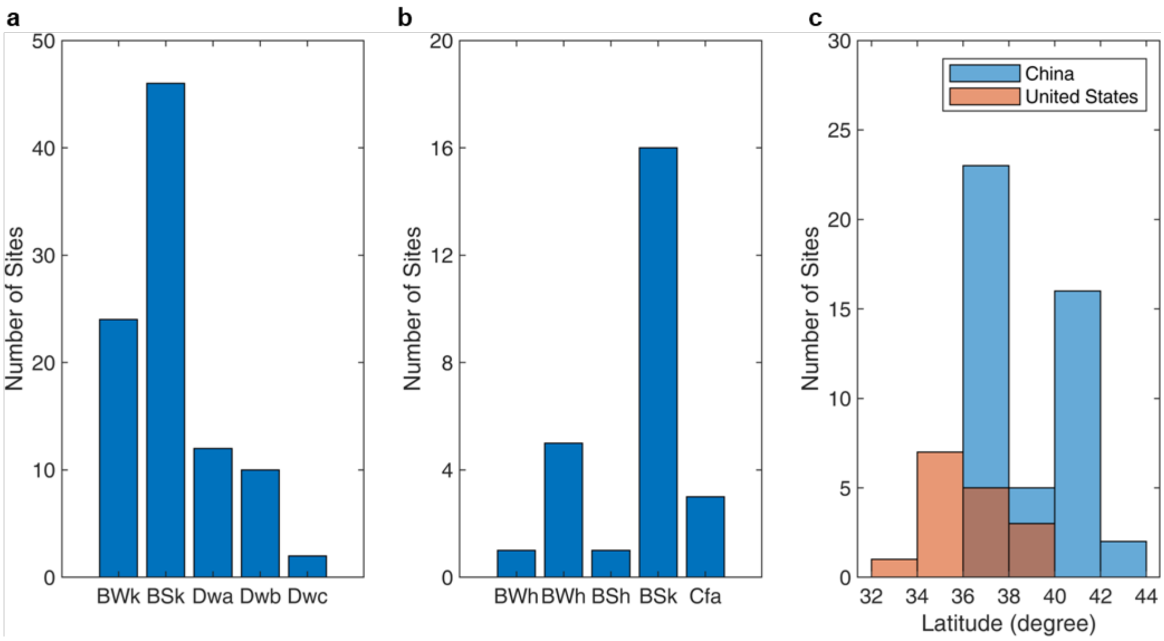

Supplementary Figure 9. The comparison of albedo change over grassland PV sites between China and the United States. a, The counts of grassland PV sites under different climate regimes in China. **b**, The counts of grassland PV sites under different climate regimes in the United States. **c**, The latitude distributions of grassland PV sites under BSk regime in China and the United States, respectively.

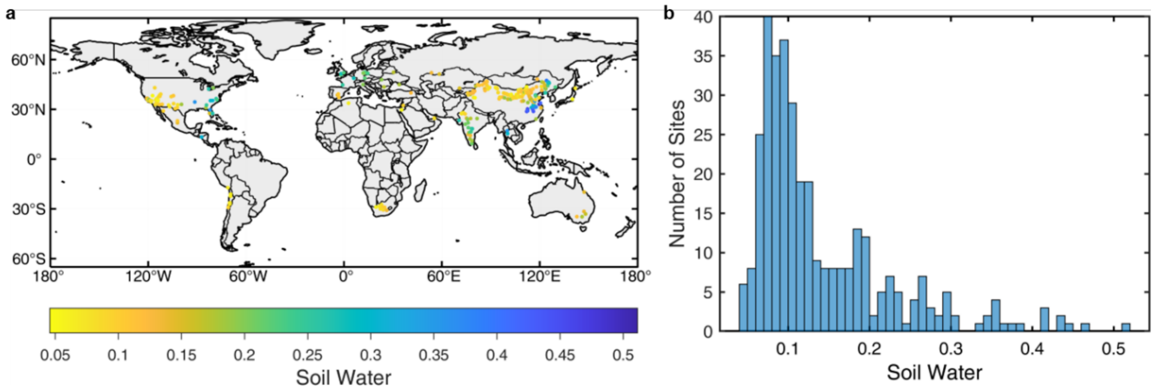

Supplementary Figure 10. The averaged soil water content of the 352 PV sites. a, Spatial pattern of sites' averaged soil water content. **b**, The histogram of corresponding mean soil water content in the 352 PV sites.

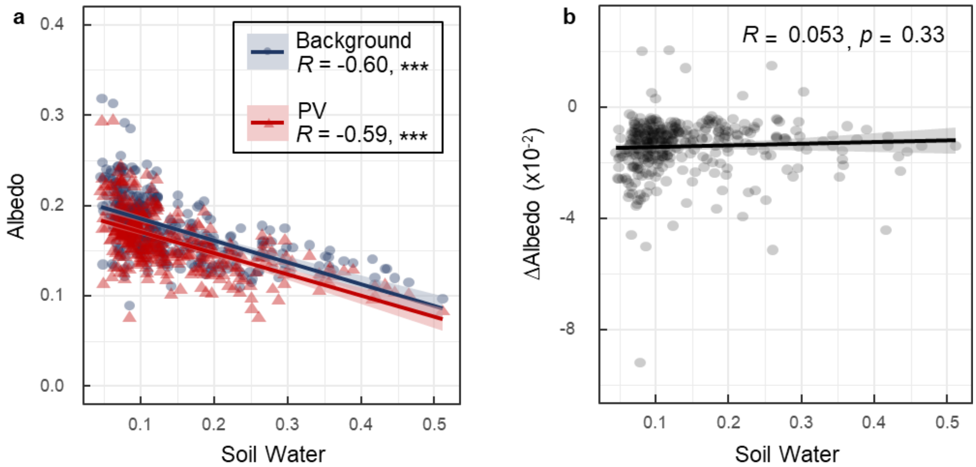

Supplementary Figure 11. The influence of soil water content on background albedo and albedo change. a, The correlation between site-level mean soil water and the albedo before (blue dots) and after (red dots) PV deployment. **b**, The relationship between soil water and albedo change.

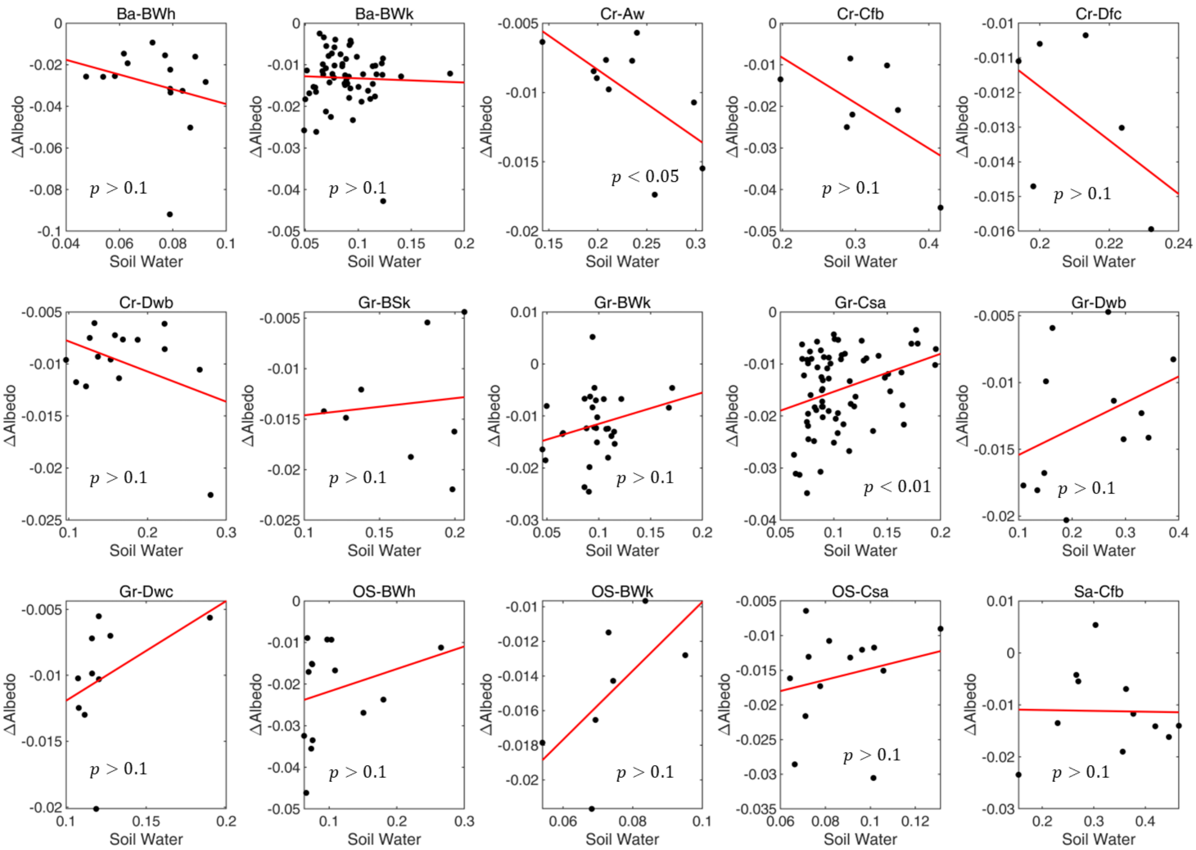

Supplementary Figure 12. The influence of soil water content on albedo change specific to different climate regimes of corresponding land-cover types.

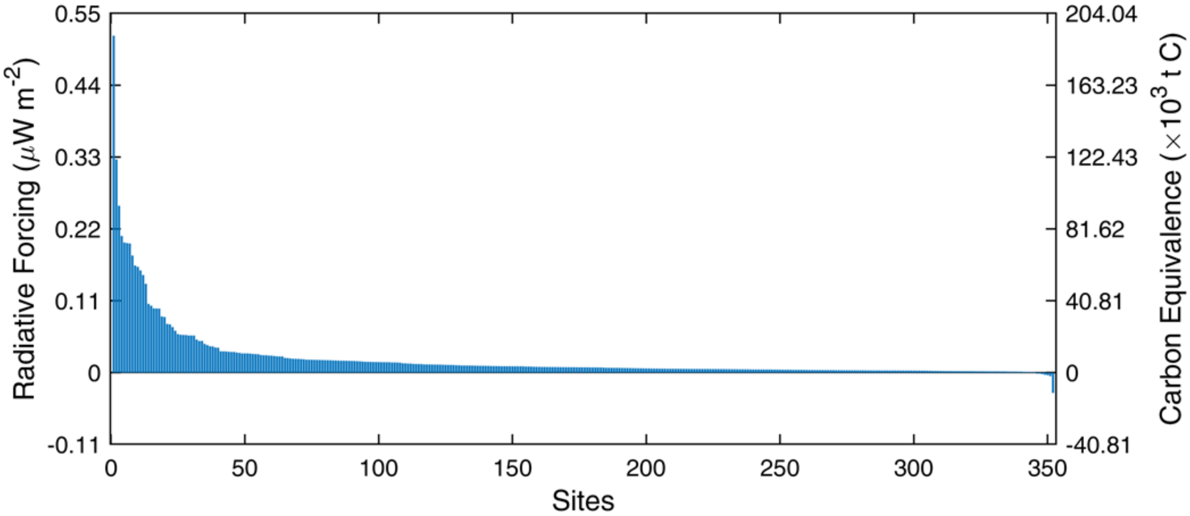

Supplementary Figure 13. The radiative forcing and carbon equivalence of different sites (352). Sites have been rearranged in descending order of radiative forcing values, from the highest to the lowest.

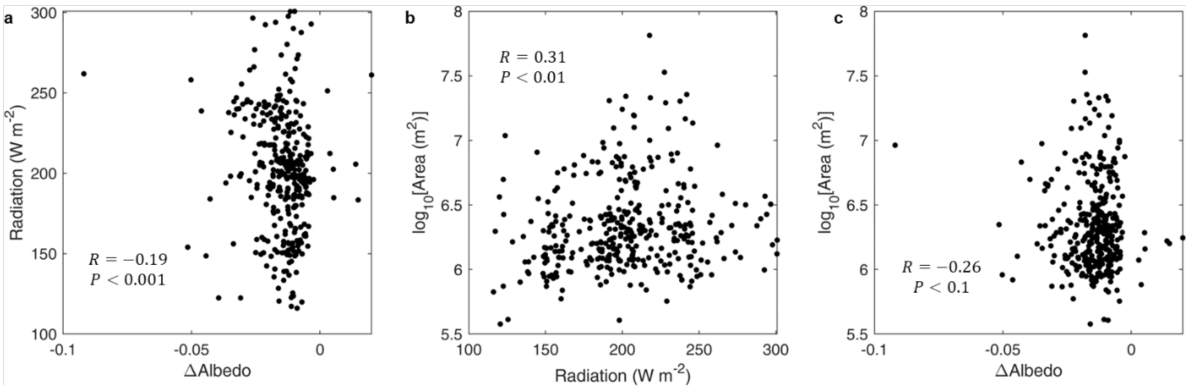

Supplementary Figure 14. The relationships between any two of the three factors: the area covered by PV panels, the albedo change caused by PV deployment, and the total downward shortwave radiation in the region. Spearman correlation analysis is used here. The three variables potentially interact with each other in pairs.

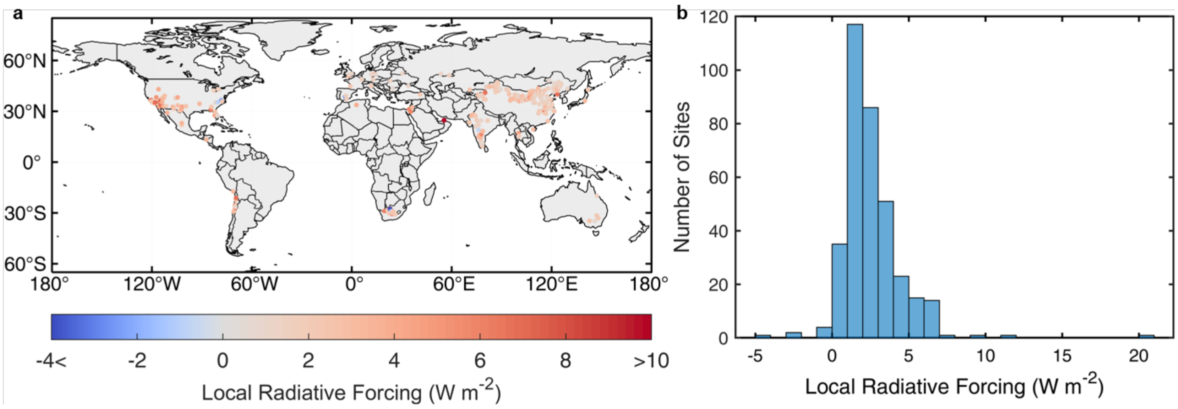

Supplementary Figure 15. The local radiative forcing (RF) of the 352 PV sites. a, Spatial pattern of sites' local RF. **b**, The histogram of corresponding local RF in the 352 PV sites.

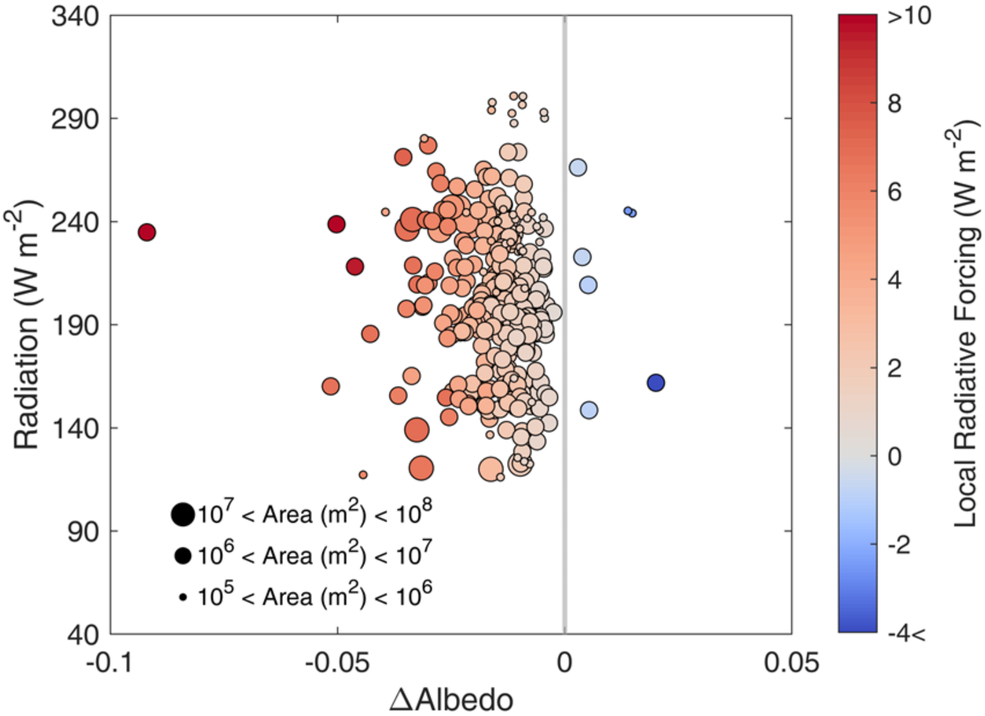

Supplementary Figure 16. Drivers influencing local radiative forcing (local RF). The grey line shows the zero value of albedo change. The greater the deviation from the zero line, the more significant the change in shortwave forcing, highlighting the dominant role of albedo change compared to radiation.

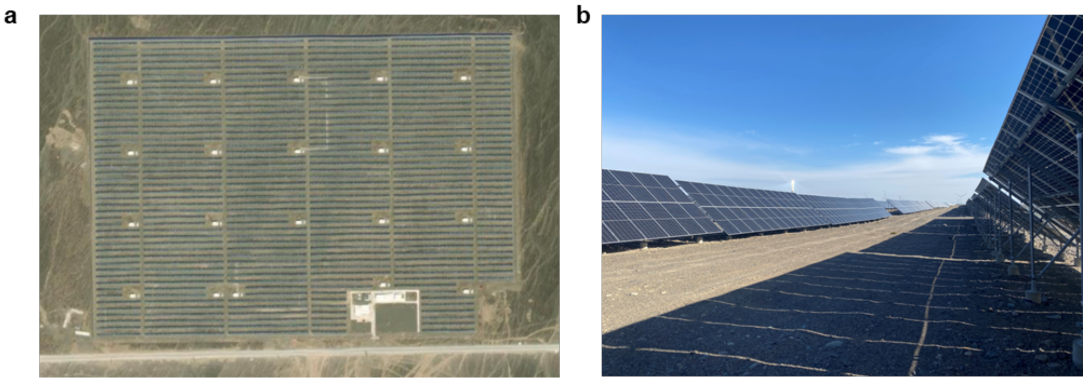

Supplementary Figure 17. A solar power plant (94.93°E, 43.60°N) in Hami City, Xinjiang, China. a, The satellite imagery extracted from ERSI World Imagery (2022-1-12) in ArcMap 10.8. **b**, A photo taken during an on-site investigation. We can find that there are large gaps between solar panel arrays in the solar farm, which is not obvious in the satellite imagery.

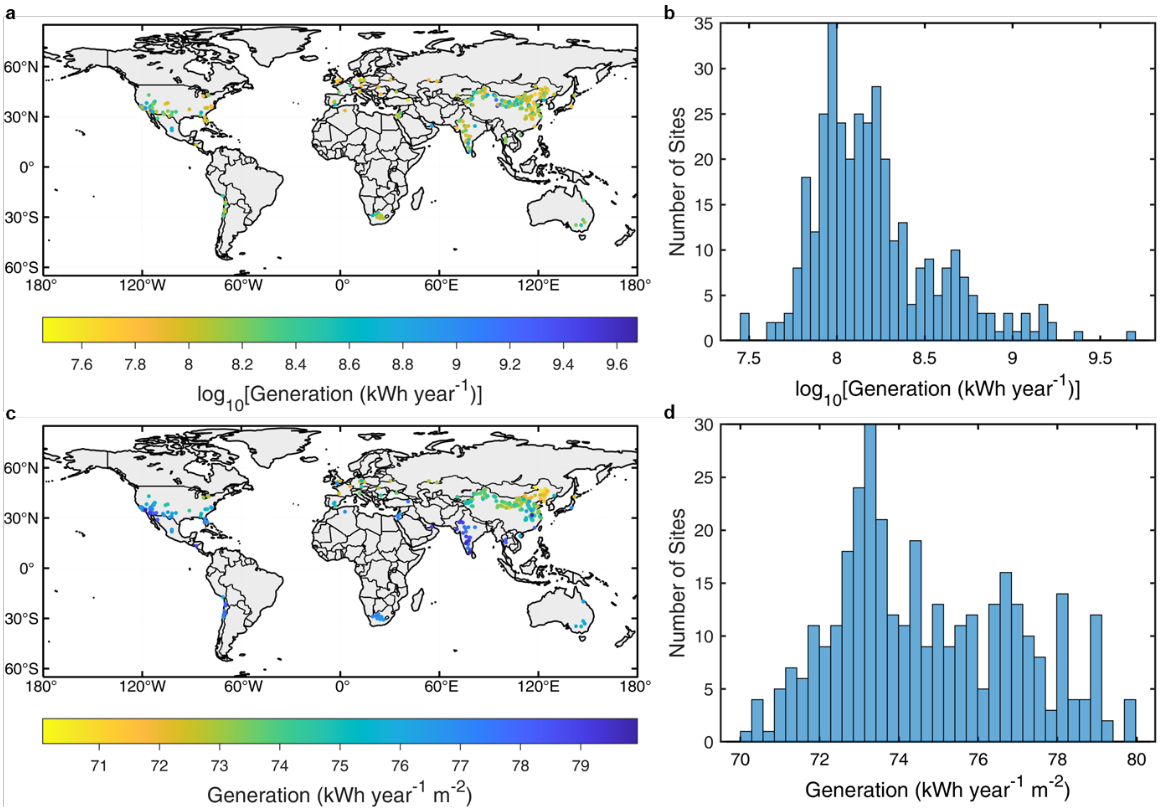

Supplementary Figure 18. The yearly total generation and generation per unit of each PV site. **a** and **b** show the spatial pattern and histogram of the total generation per PV site, while **c** and **d** show the generation per unit of each PV site.

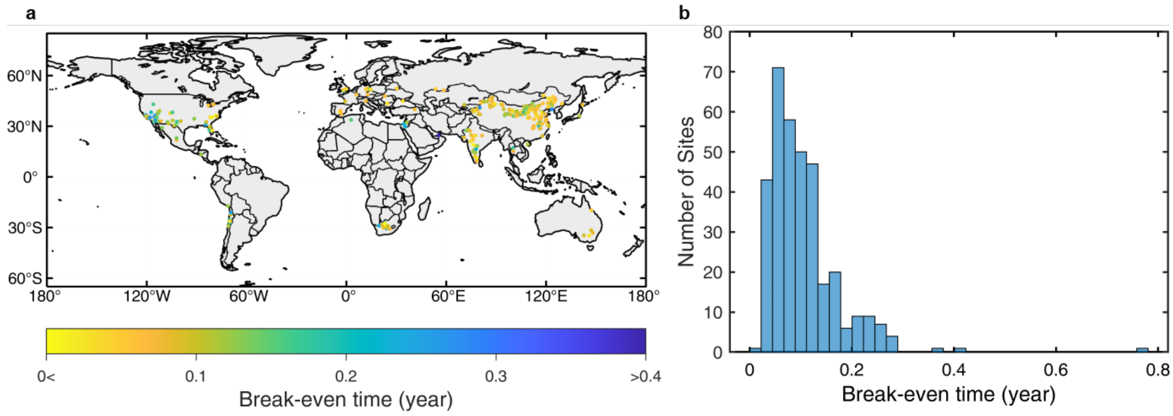

Supplementary Figure 19. The break-even time of each PV site. a, Spatial pattern of sites' break-even time. **b**, The frequency distribution histogram of PV sites' break-even time. Only positive values are shown.

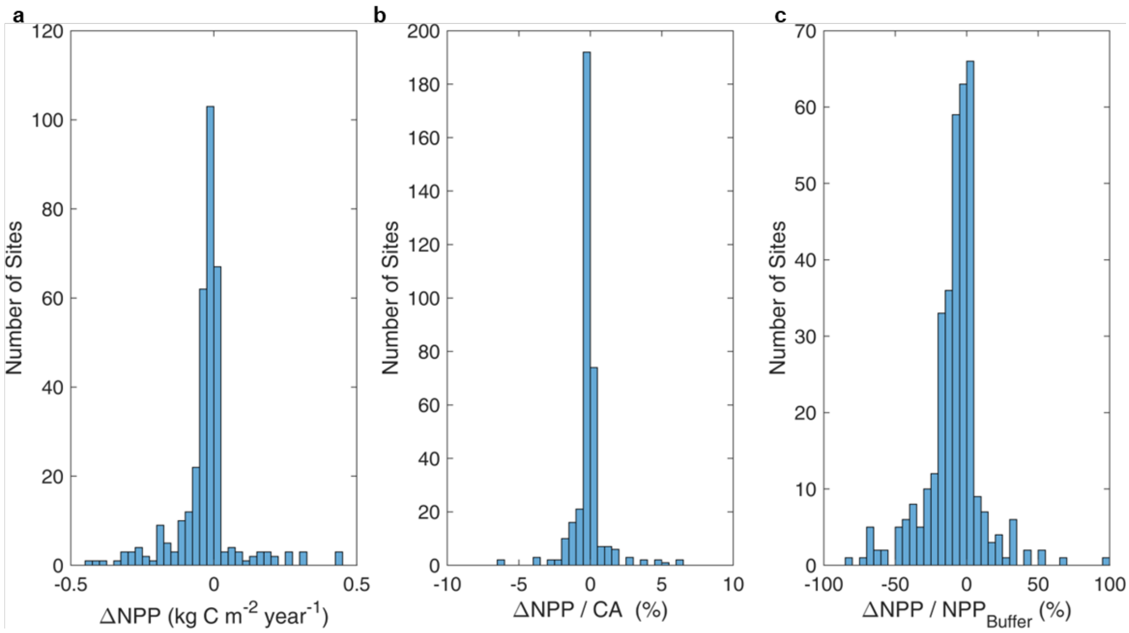

Supplementary Figure 20. The influence of PV installation on Net Primary Productivity (NPP). a, The NPP difference between the PV site and the corresponding buffer zone. **b**, The comparison between the changed NPP and carbon avoidance (CA; Supplementary Methods) by PV generation. **c**, The ratio of NPP change value to the buffer zone's NPP.

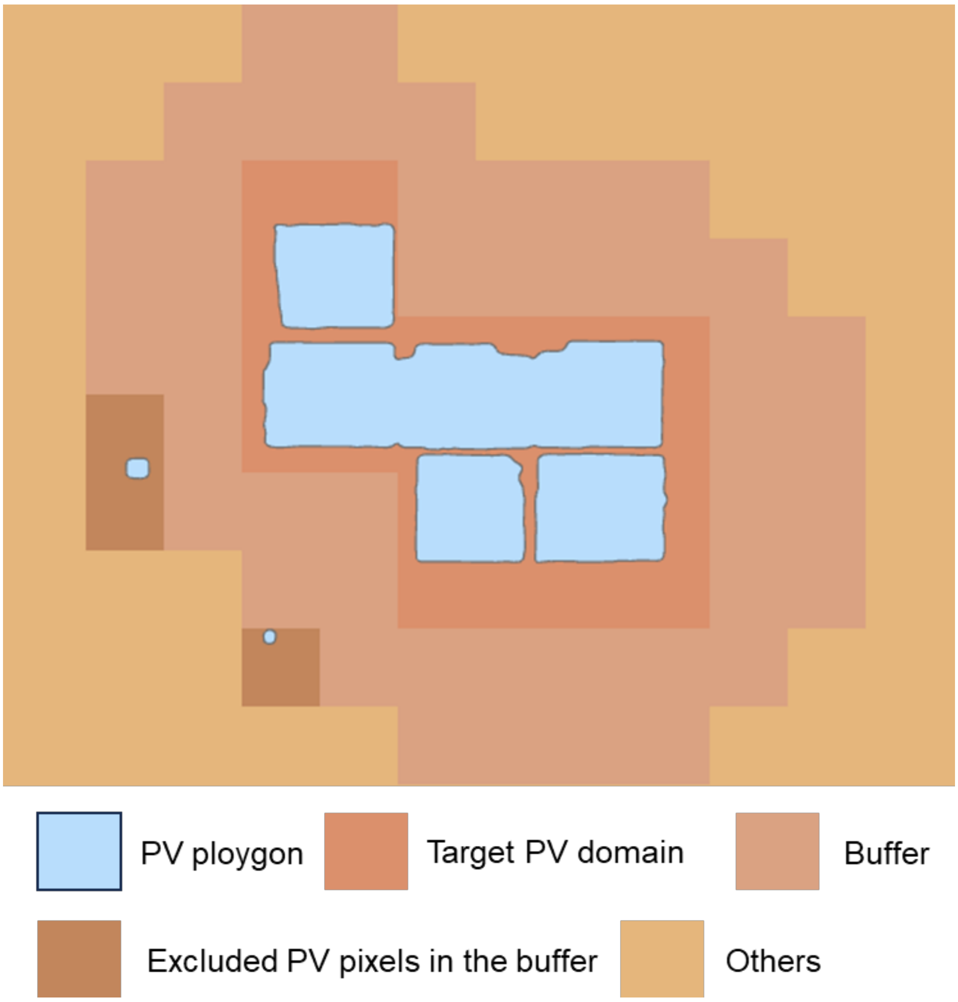

Supplementary Figure 21. The diagram of creating a buffer near a target PV domain (site). To create a buffer zone with a width of 2 pixels around a selected PV connected region, a dilation operation is used to enlarge the target PV region by adding two pixels around its edges. Any other PV regions within the buffer zone, apart from the target PV domain, are excluded.

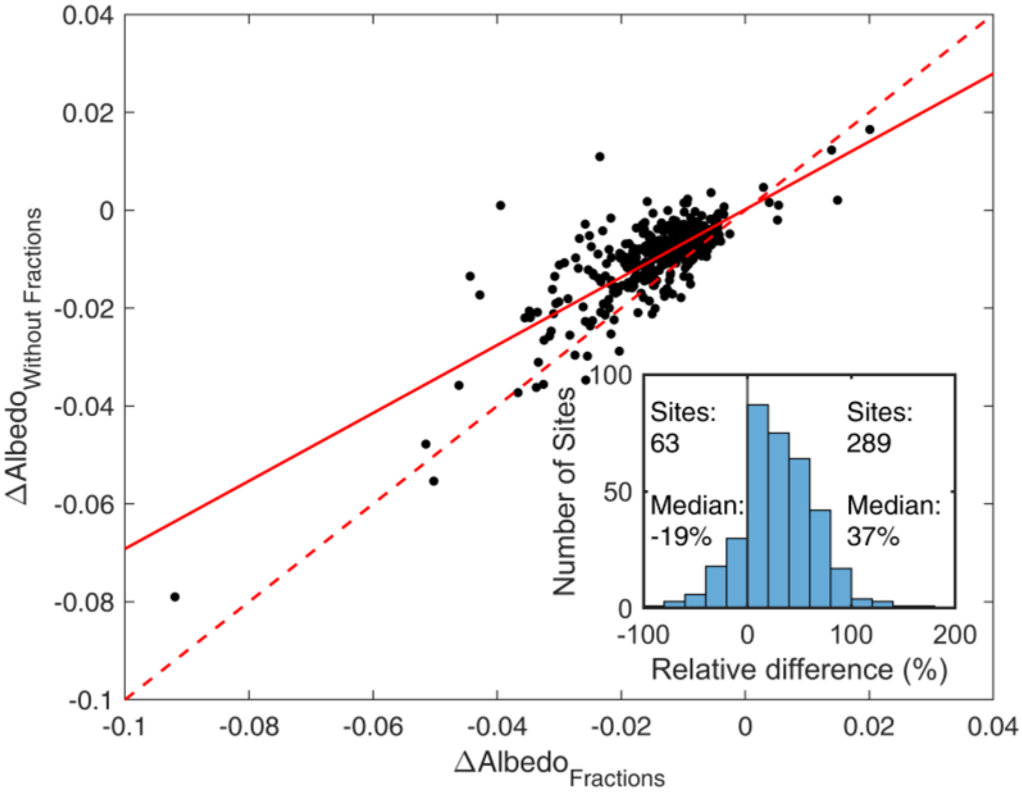

Supplementary Figure 22. The comparison of absolute albedo change (ΔAlbedo) over 352 selected PV sites between considering the PV grid fractions and without considering the fractions. The red solid line represents the line of equality (x=y), while the dashed line indicates the fitting line. The inset details the ratio of differences in albedo change with and without PV grid fractions to albedo change with PV grid fractions. A relative difference greater than zero indicates that the albedo change is greater when considering PV grid fractions. Additionally, the inset captions provide the count of sites with relative differences both greater and less than zero, along with their respective median relative difference values.

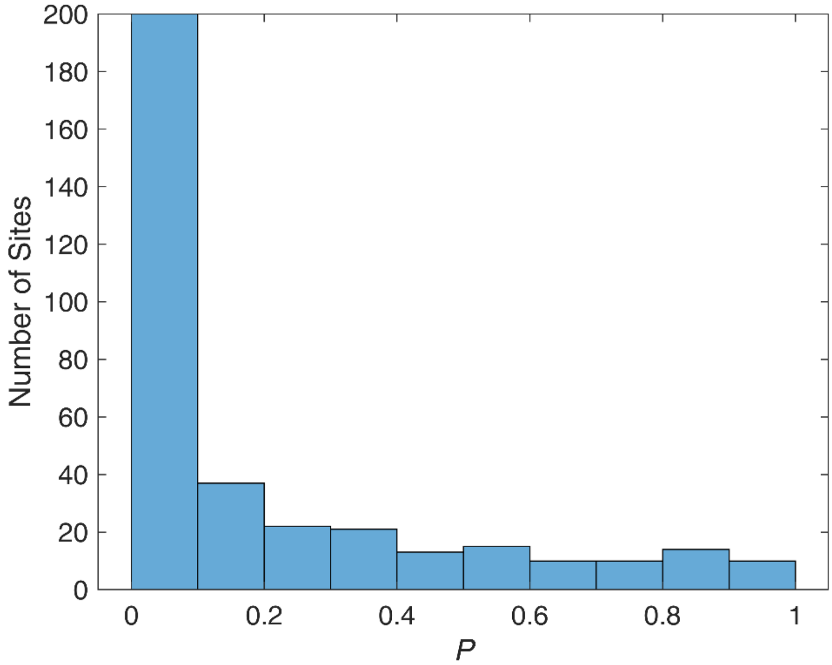

Supplementary Figure 23. The histogram of *P* values when utilizing our linear parameterization method for calculating NPP changes over 352 sites. Nearly half of the sites have *P* values greater than 0.1.

Supplementary References

1. Stern, R., et al., 2023. Photovoltaic fields largely outperform afforestation efficiency in global climate change mitigation strategies. *Proceedings of the National Academy of Sciences Nexus*. **2**, pgad352.
2. Li, Y., et al., 2018. Climate model shows large-scale wind and solar farms in the Sahara increase rain and vegetation. *Science*. **361,** 1019-1022.
3. Lu, Z., et al., 2021. Impacts of Large-Scale Sahara Solar Farms on Global Climate and Vegetation Cover. *Geophysical Research Letters.* **48**, e2020GL090789.
4. Millstein, D., et al., 2011. Regional climate consequences of large-scale cool roof and photovoltaic array deployment. *Environmental Research Letters*. **6**, 034001
5. Chang, R., et al., 2020. Simulated local climatic impacts of large-scale photovoltaics over the barren area of Qinghai, China. *Renewable Energy*. **145,** 478-489.
6. Chang, R., et al., 2022. A coupled WRF-PV mesoscale model simulating the near-surface climate of utility-scale photovoltaic plants. *Solar Energy*, 245, 278–289.
7. Yang, L., et al., 2017. Study on the local climatic effects of large photovoltaic solar farms in desert areas. *Solar Energy.* **144,** 244-253.
8. Chang, R., et al., 2018. Observed surface radiation and temperature impacts from the large-scale deployment of photovoltaics in the barren area of Gonghe, China. *Renewable Energy*. **118,** 131-137.
9. Broadbent, A. M., et al., 2019. The Observed Effects of Utility-Scale Photovoltaics on Near-Surface Air Temperature and Energy Balance. *Journal of Applied Meteorology and Climatology*. **58,** 989-1006.
10. Li, P., et al., 2022. Physical analysis of the environmental impacts of fishery complementary photovoltaic power plant. *Environmental Science and Pollution Research*. **29,** 46108-46117.
11. Li, Z., et al., 2022. A comparative study on the surface radiation characteristics of photovoltaic power plant in the Gobi desert. *Renewable Energy*. **182,** 764-771.
12. Ying, J., et al.,2022. The characteristics and parameterizations of the surface albedo of a utility-scale photovoltaic plant in the Gobi Desert. *Theoretical and Applied Climatology.* **151**, 1469-1481.
13. Hua, Y., et al., 2022. The Influences of the Desert Photovoltaic Power Station on Local Climate and Environment: A Case Study in Dunhuang Photovoltaic Industrial Park, Dunhuang City, China in 2019. *Atmosphere*. **13,** 1235.

14. Zhang, X., et al, 2020. Assessing the Effects of Photovoltaic Powerplants on Surface Temperature Using Remote Sensing Techniques. *Remote Sensing.* **12**, 1825.
15. Xu, Z., et al., 2024. A global assessment of the effects of solar farms on albedo, vegetation, and land surface temperature using remote sensing. *Solar Energy*. **268**, 112198.
16. Beck, H., et al, 2018. Present and future Köppen-Geiger climate classification maps at 1-km resolution. *Scientific Data*. **5**, 180214.